Final Report
Out-Reach In-Space Technology Experiments Program
Contract Number NAS8-37754
Control of Flexible Robot Manipulators in Zero Gravity
Experiment Definition Phase
August 16, 1988 through August 15, 1989

by
Warren F. Phillips

UTAH STATE UNIVERSITY
CENTER FOR COMPUTER-AIDED DESIGN AND MANUFACTURING
Logan, Utah 84322-4130
Phone: (801) 750-2950

1. Introduction

The control systems used in today's industrial robots are all based on the assumption of rigid links. In order to force manipulators to conform to the rigid link model, today's industrial robots are all built with very stiff and massive links. This results in a very high robot to payload weight ratio. A survey of industrial robots on the market today shows the average robot to payload weight ratio is about 50. The high cost of placing mass in space makes this weight a significant drawback in using robots of this design in space.

When conventional control systems such as those used in today's industrial robots are used to control lightweight robots with flexible links, large elastic vibrations are induced in the robot links. These vibrations make it very difficult to perform tasks quickly with such robots. The solutions being used today are to either move the robot very slowly or to wait a long time between moves to allow the induced vibrations to damp out.

The development of a manipulator control system capable of accurately controlling a robot with lightweight flexible links in zero gravity is of prime importance to the efficient utilization of robot manipulators in space. Because such a manipulator control system makes use of the simplification which results from ignoring gravitational forces, it would not work well in the presence of gravity. Thus, in-space experiments are required to verify and improve such a control system.

An in-space experiment is being developed to test the feasibility of accurately controlling robot manipulators with lightweight, non-rigid links. The objective of the experiment definition phase of this study was to develop and ground test a control system which would minimize induced vibrations in these flexible link robots. The control system that was developed in this study looks very promising. In all of the testing done to date, we were able to eliminate the induced vibrations without increasing response time.

This new control system was tested in two ways. First, a computer simulation of a flexible link robot arm in zero gravity was written. The robot arm was simulated using both a conventional robot control system and the new flexible link control system. Secondly, a working model of a two axis robot arm with flexible links was constructed and ground tested using both conventional control and the new control system. Agreement between the simulation and the experiment was excellent. However, to minimize the effects of gravity in the ground testing, it was necessary study only two-dimensional motion in the plane normal to gravity.

To fully evaluate this new control system in three dimensions, a three axis robot arm will need to be tested in zero gravity. Based on the results of the computer simulation and ground testing carried out during this phase of the study, an in-space experiment will be proposed to test the new control system on a three-axis robot in zero gravity.

2. The Test Arm

For the purpose of ground testing it was necessary to construct a robot arm with links that would exhibit significant deflection as a result of inertial loading but negligible deflection as a result of gravitational loading. To accomplish this, the two axis arm shown in Figure 1 was designed and constructed. This robot has two revolute joints both moving their respective links in the horizontal plane. The links were constructed to be flexible in the horizontal direction but rigid in the vertical direction. This design is intended to minimize the effects of gravity in the ground tests. Each link is driven by a Baldor model MTE-4090-B DC servo motor, controlled using a Galil model DMC-200 controller and a Motion Science model HB-8016-2 MOSFET PWM amplifier.

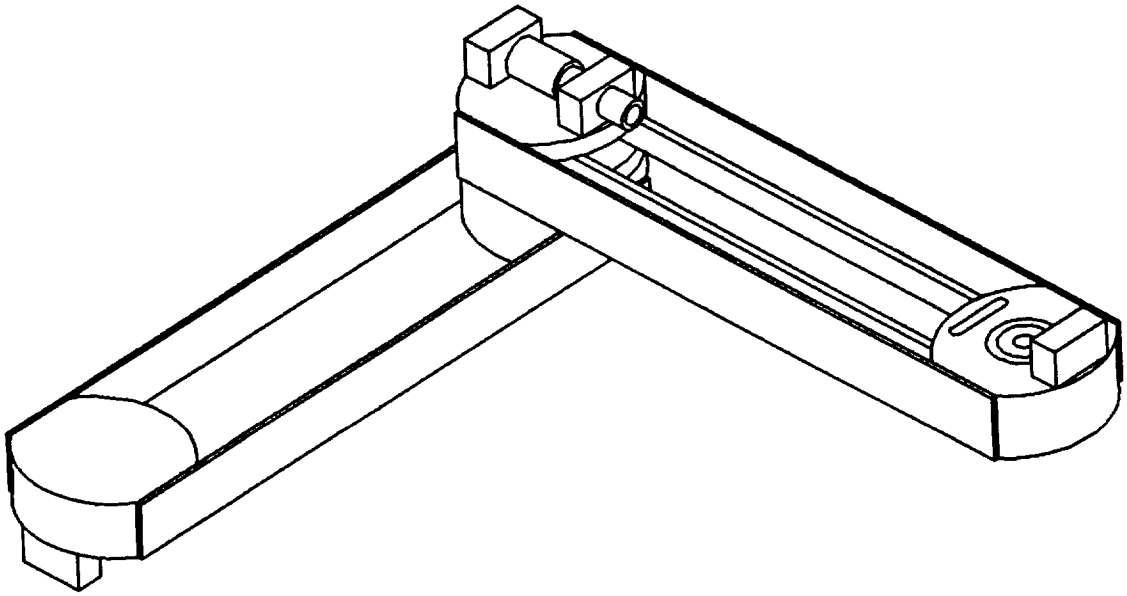

Figure 1. The experimental robot arm.

Each link of the arm was fitted with independent position and velocity sensors to provide feedback to the control loop. A Baldor model MS-3102A-24-7-P optical encoder was used for joint position feedback and a Baldor model MTE-4090-FL-3B tachometer was used to provide the joint velocity feedback. The use of optical encoders and tachometers to provide position and velocity feedback in robot control is well documented in the literature and will not be discussed further in this report.

In addition to these usual position and velocity feedback sensors, the test arm was also fitted with a deflection feedback sensor. For this purpose a silicon photodiode position sensor made by Silicon Detector Corporation was used. These sensors are designed so that when a spot of light illuminates a region of the active area of the cell, an output voltage can be produced that is linearly proportional to the position of the spot along the axis of the cell. The detector used for the deflection sensor is shown in Figure 2. This device is used to precisely measure the location of an optical image with respect to a specified system reference point.

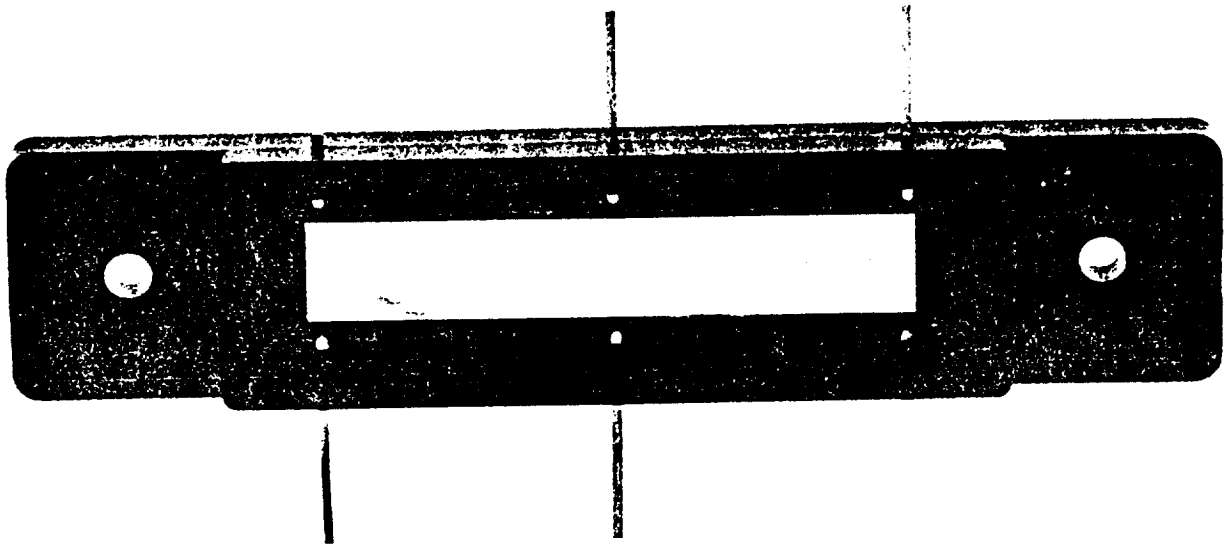

Figure 2. The silicon photodiode detector used in the deflection sensor.

Such detectors are noted for their wide dynamic range. They achieve very accurate analog position measurement over relatively large areas. The response of these detectors is not influenced by the size or shape of the light image as long as this image remains within the active area of the detector. Moreover, operation far from the optical center or null point does not impair accuracy.

The difference between detectors of this type and other photodetectors is that a signal current does not flow through the silicon chip to be collected at the back side. The current flows laterally until collected at ohmic contacts located at the edges of the active area. When a spot of light illuminates a region of the active area, a small forward bias is induced at the illuminated region. This forward bias causes ohmic currents to flow to each of the collecting contacts. The fraction of the total signal current collected at each contact is proportional to the conductance from the point of illumination to that contact. Since the substrate conductance between the spot and a given cathode is inversely proportional to the distance between the spot and that cathode, a signal can be obtained that is proportional to the displacement of the spot from the central axis.

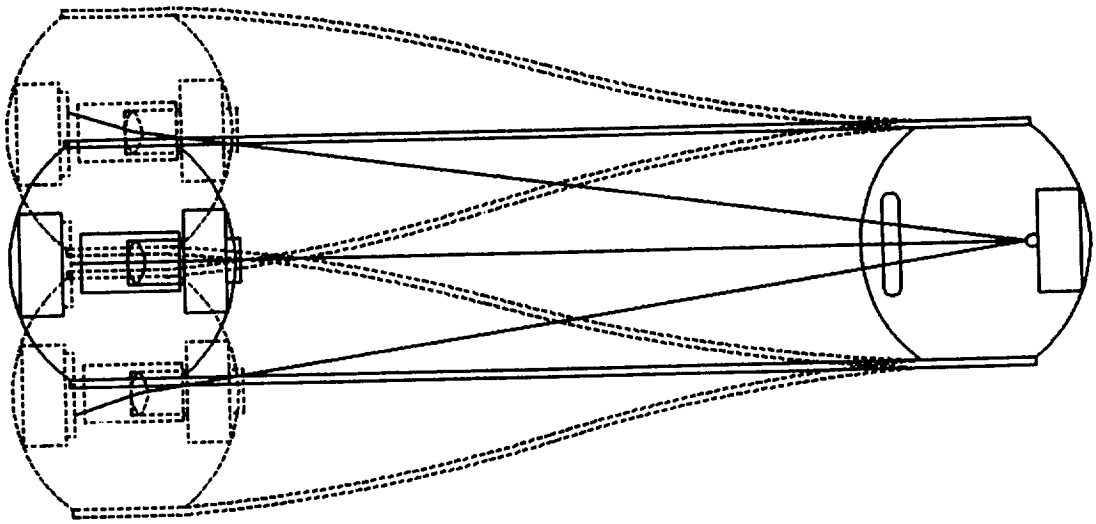

Figure 3. The deflection sensor mechanism.

To use this detector as a deflection sensor, a small light source was placed at the base of each link and the detector was placed at the tip of the link. A lens was used to focus an image of the light source on the detector. Deflection of the link would cause the image of the source to move across the active area of the detector, as shown in Figure 3, producing an output voltage proportional to the deflection.

For the arm control system, an interface board for each joint was designed and built to link the DC motors and all of the sensors to an IBM PC computer. All of the control computations were done in software so they could easily be modified to test different control algorithms. Figure 4 shows a block diagram of the each control loop. The completed arm with the deflection sensors in place is shown in Figure 5.

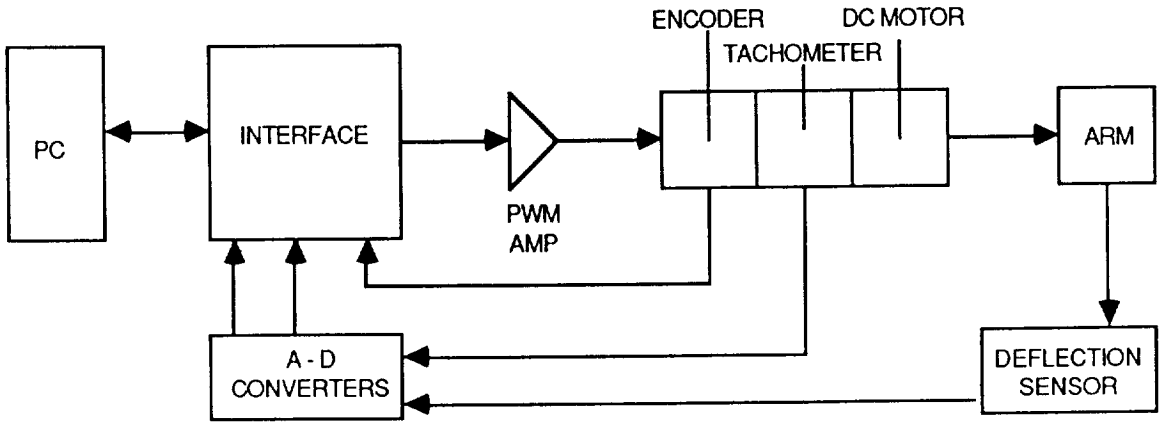

Figure 4. Block diagram of the control loop.

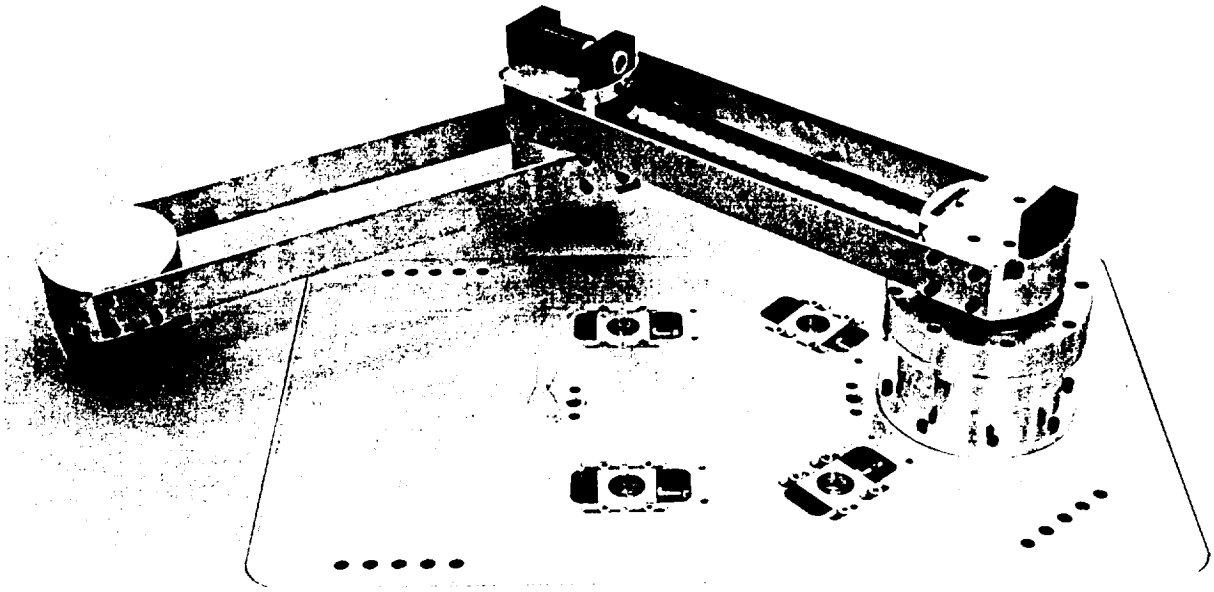

Figure 5. The completed arm.

3. The Computer Simulation

Applying Lagrangian mechanics to the robot arm described in section 2, we obtain a relationship between, the torques applied at each axis and the angular displacement of the two links. This results in

$$T_1 = [\, I_1 + 2I_2(1 + \cos\theta_2)\,]\,(\ddot{\theta}_1 - \ddot{\delta}_1/R) + [\, I_2(1 + \cos\theta_2)\,]\,(\ddot{\theta}_2 - \ddot{\delta}_2/R) - (I_2 \sin\theta_2)\,(\dot{\theta}_2 - \dot{\delta}_2/R)^2 - (I_2 \sin\theta_2)\,(\dot{\theta}_1 - \dot{\delta}_1/R)\,(\dot{\theta}_2 - \dot{\delta}_2/R) \quad (1)$$

$$T_2 = [\, I_2(1 + \cos\theta_2)\,]\,(\ddot{\theta}_1 - \ddot{\delta}_1/R) + I_2\,(\ddot{\theta}_2 - \ddot{\delta}_2/R) + (I_2 \sin\theta_2)\,(\dot{\theta}_1 - \dot{\delta}_1/R)^2 \quad (2)$$

where T is joint torque, I is the link moment of inertia, θ is angular joint displacement, δ is link deflection, R is link length, the subscripts 1 and 2 refer to the first and second link respectively and a dot signifies differentiation with respect to time. The first two terms in equation (1) result from angular acceleration, the third term results from centrifugal acceleration and the last term is the result of Coriolis acceleration.

The torque applied to each joint is related to the voltage applied to each actuator by

$$T_1 = K_1 E_1 - A_1 \ddot{\theta}_1 - C_1 \dot{\theta}_1 \quad (3)$$

$$T_2 = K_2 E_2 - A_2 \ddot{\theta}_2 - C_2 \dot{\theta}_2 \quad (4)$$

where K is a proportionality constant, E is the voltage applied to the actuator, A is the output inertia of actuator and drive train and C is the output damping coefficient for the actuator and drive train. From the theory of elasticity, the joint torques are also related to the link deflections by the equations

$$T_1 = I_1\omega_1^2 \delta_1/R - .5I_2\omega_2^2 \delta_2/R \quad (5)$$

$$T_2 = I_2\omega_2^2 \delta_2/R \quad (6)$$

where ω is the natural frequency of the link.

Equations (1) through (6) provide a nonlinear system that can be solved for the six unknowns, which are the joint displacements, the joint torques and the link deflections, in terms of the voltage applied to the two actuators. The initial conditions to be used with this system are

$$\dot{\theta}_1(0) = 0 \quad (7)$$

$$\dot{\theta}_2(0) = 0 \quad (8)$$

$$\theta_1(0) = \theta_{10} \quad (9)$$

$$\theta_2(0) = \theta_{20} \quad (10)$$

$$\dot{\delta}_1(0) = 0 \quad (11)$$

$$\dot{\delta}_2(0) = 0 \quad (12)$$

$$\delta_1(0) = 0 \quad (13)$$

$$\delta_2(0) = 0 \quad (14)$$

where θ_{10} and θ_{20} are the initial position of the first and second joints respectively.

The simulations carried out in this study were obtained from numerical solutions to equations (1) through (6), subject to the initial conditions given in equations (7) through (14). The actuator voltages were computed from the output variables with different control algorithms using a one millisecond sample time.

The control algorithm used in most conventional robot control systems is given by

$$K_1 E_1 = P_1 (\theta_{d1} - \theta_1) - V_1 \dot{\theta}_1 \quad (15)$$

$$K_2 E_2 = P_2 (\theta_{d2} - \theta_2) - V_2 \dot{\theta}_2 \quad (16)$$

where θ_d is the desired joint angle, P is the position feedback gain and V is the velocity feedback gain. With control systems of this type, the magnitude of the velocity feedback gain is chosen to prevent control oscillations and the position feedback gain is chosen as large as possible without inducing significant structural oscillations. This control system works well for robots with stiff links. However, if the links are flexible, the avoidance structural oscillations requires a position feedback gain so low that the response time is not adequate for most applications.

After testing many different control algorithms with the computer simulation, it was found that the structural oscillations could be prevented without increasing response time by simply adding a deflection feedback term to the conventional control algorithm. This results in

$$K_1 E_1 = P_1 (\theta_{d1} - \theta_1) - V_1 \dot{\theta}_1 - D_1 \delta_1 \quad (17)$$

$$K_2 E_2 = P_2 (\theta_{d2} - \theta_2) - V_2 \dot{\theta}_2 - D_2 \delta_2 \quad (18)$$

where D is the deflection feedback gain.

In the results that follow, the control algorithm given by equations (15) and (16) will be referred to as the conventional control system and the control algorithm given by equations (17) and (18) will be referred to as the new control system.

4. Results

The results of the ground testing are summarized in Figures 6 through 17. These are representative samples of the results obtained in this phase. Many other conditions were also tested but the results were very similar and will not be included in this report

The results shown in Figure 6 are the link position as a function of time as predicted by the computer simulation using a conventional overdamped robot control system with only position and velocity feedback. Figure 7 shows the results obtained when this control system was implemented on the test robot. The induced vibrations are very apparent in both figures and the agreement between simulation and experiment is excellent.

Figure 8 shows the results obtained when the same robot as that shown in Figure 6 was simulated using the new control system which uses deflection feedback as well as position and velocity feedback in the control loop. Figure 9 shows the

results obtained when this control system was implemented on the test robot. Notice that in both the simulation and the experiment the induced vibrations are eliminated without decreasing the response time. Here again there is good agreement between the simulation and the experimental results.

Figure 10 shows the link deflection as a function of time that resulted when the tip of the link on the test robot was was deflected by a sudden impact. During this test the link position was being controlled by the conventional control system using only position and velocity feedback. Figure 11 shows the results of the same test when position was being controlled by the new control system with deflection feedback. Notice that this control system was able to very quickly damp out the vibrations caused by the impact.

Figure 12 shows a simulation of a typical joint movement on the two axis arm when controlled by the conventional control system. Notice the multiple modes of vibration induced by this control system. Figure 13 shows a simulation for the same joint movement on the same robot when controlled by the new control system. As can be seen, all modes of vibration are eliminated with no decrease in response time.

Figure 14 shows a typical joint movement on the two axis test arm when controlled by the conventional control system. Figure 15 shows the same joint movement on the test robot when controlled by the new control system. Here again it can be seen that all vibrations are eliminated with no decrease in response time.

Figure 16 shows the link deflection as a function of time that resulted when the tip of the second link on the test robot was was deflected by a sudden impact. During this test the link position was being controlled by the conventional control system using only position and velocity feedback. Figure 17 shows the results of the same test when position was being controlled by the new control system with deflection feedback. Notice that here again this control system was able to very quickly damp out the vibrations in both links that were caused by the impact.

5. Conclusions

The results obtained in the present study show that it is possible to control light-weight robots with flexible links in a manner that produces good response time and does not induce unacceptable link vibrations. However, deflections induced by gravity cause large static position errors with such a control system. For this reason, it is not possible to use this control system for controlling motion in the direction of gravity. The control system does, on the other hand, have potential for use in space. However, in-space experiments will be needed to verify its applicability to robots moving in three dimensions.

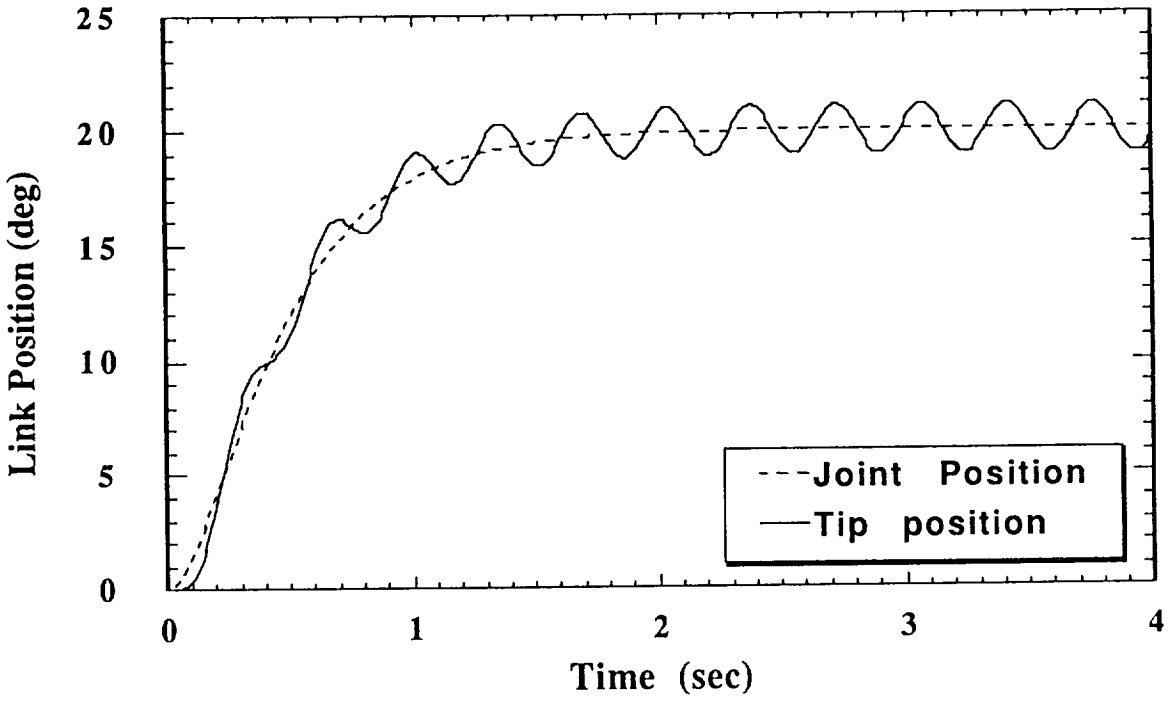

Figure 6. Simulated link position as a function of time for a 20 degree move of a single link using conventional position and velocity feedback control.

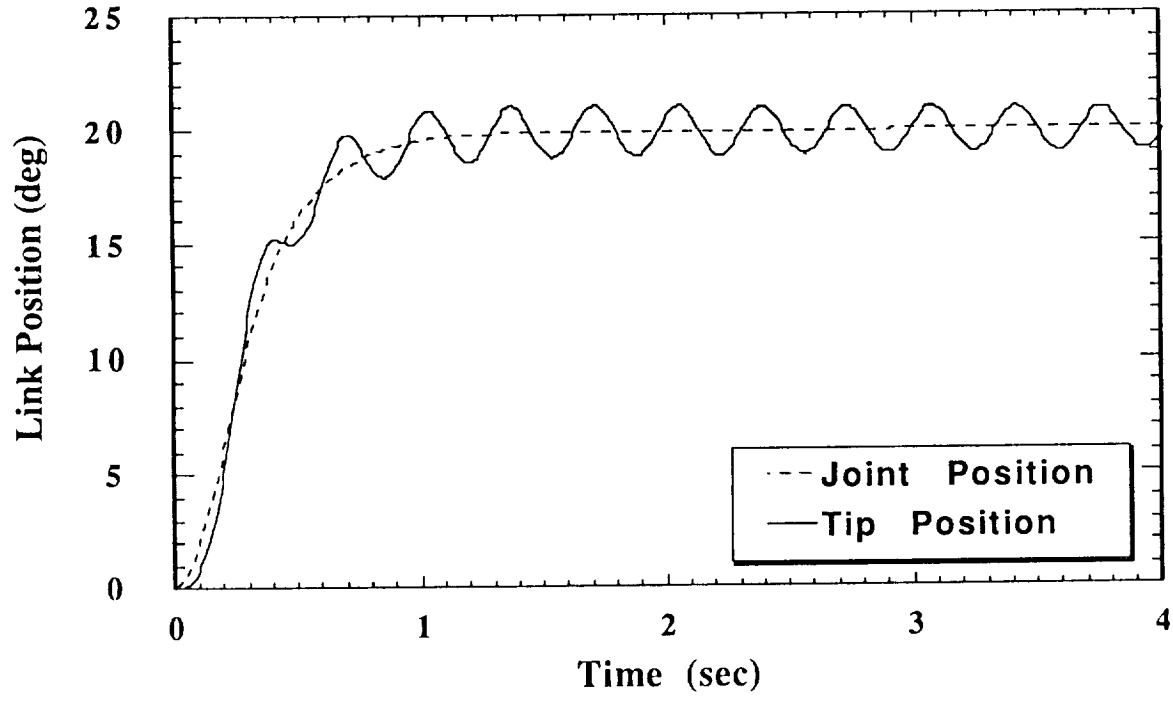

Figure 7. Experimental link position as a function of time for a 20 degree move of a single link using conventional position and velocity feedback control.

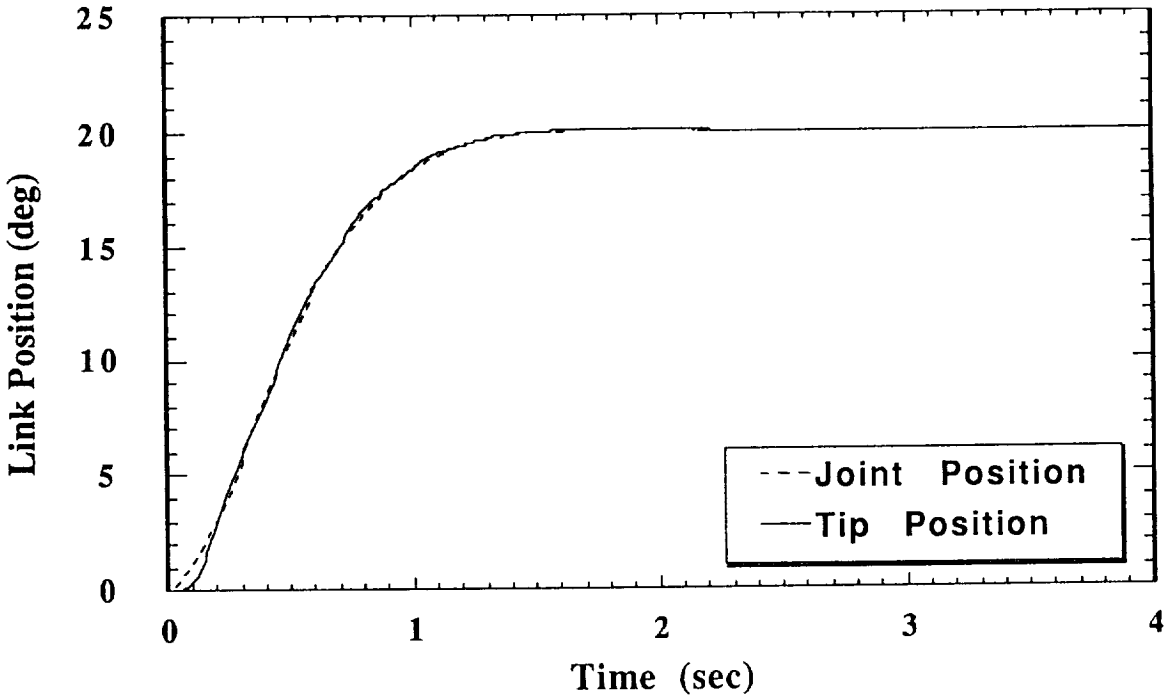

Figure 8. Simulated link position as a function of time for a 20 degree move of a single link using the new control system with deflection feedback.

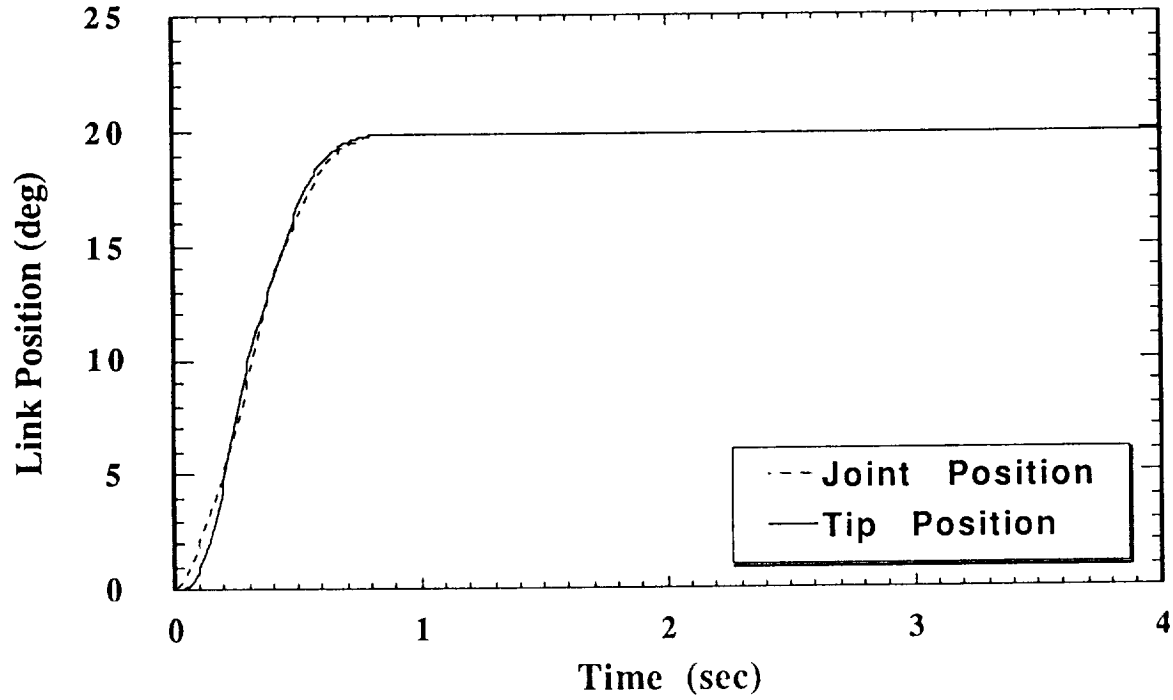

Figure 9. Experimental link position as a function of time for a 20 degree move of a single link using the new control system with deflection feedback.

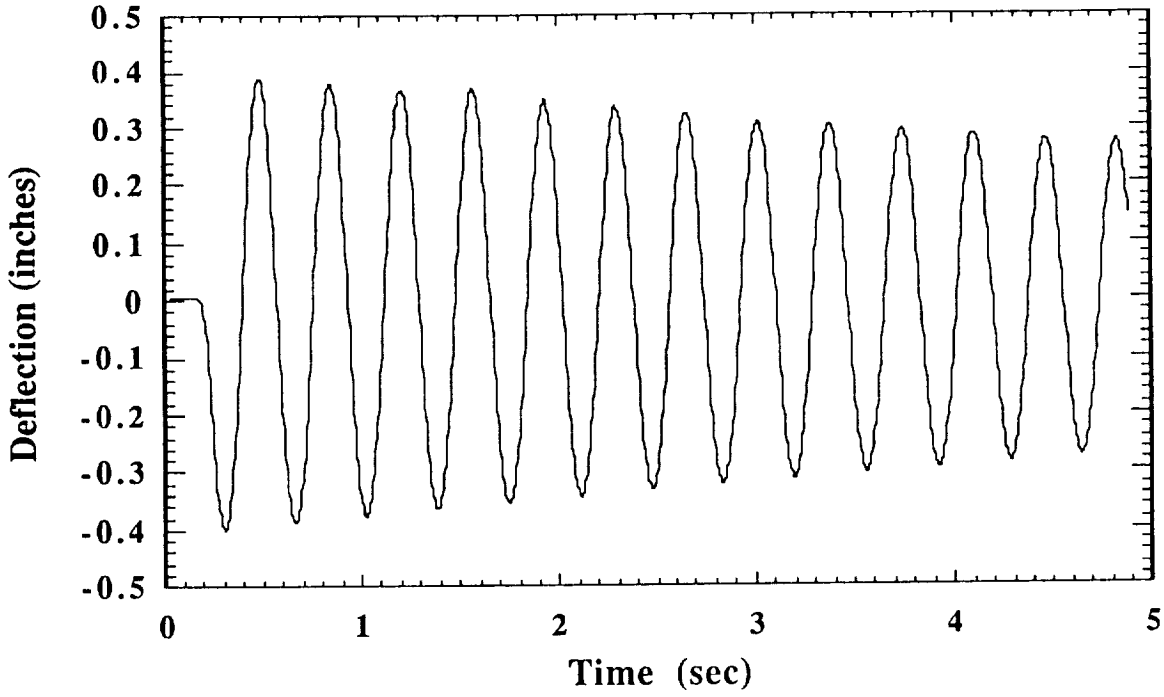

Figure 10. Experimental link deflection as a function of time for an impulse loading at the tip of a single link using conventional position and velocity feedback control.

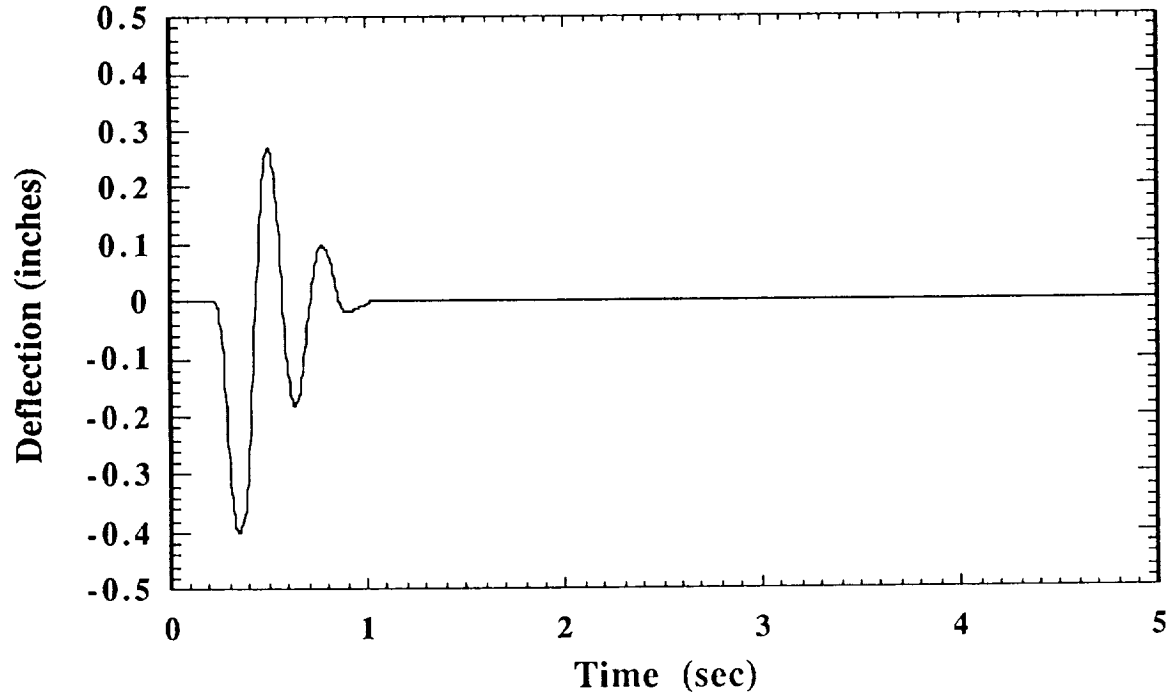

Figure 11. Experimental link deflection as a function of time for an impulse loading at the tip of a single link using the new control system with deflection feedback.

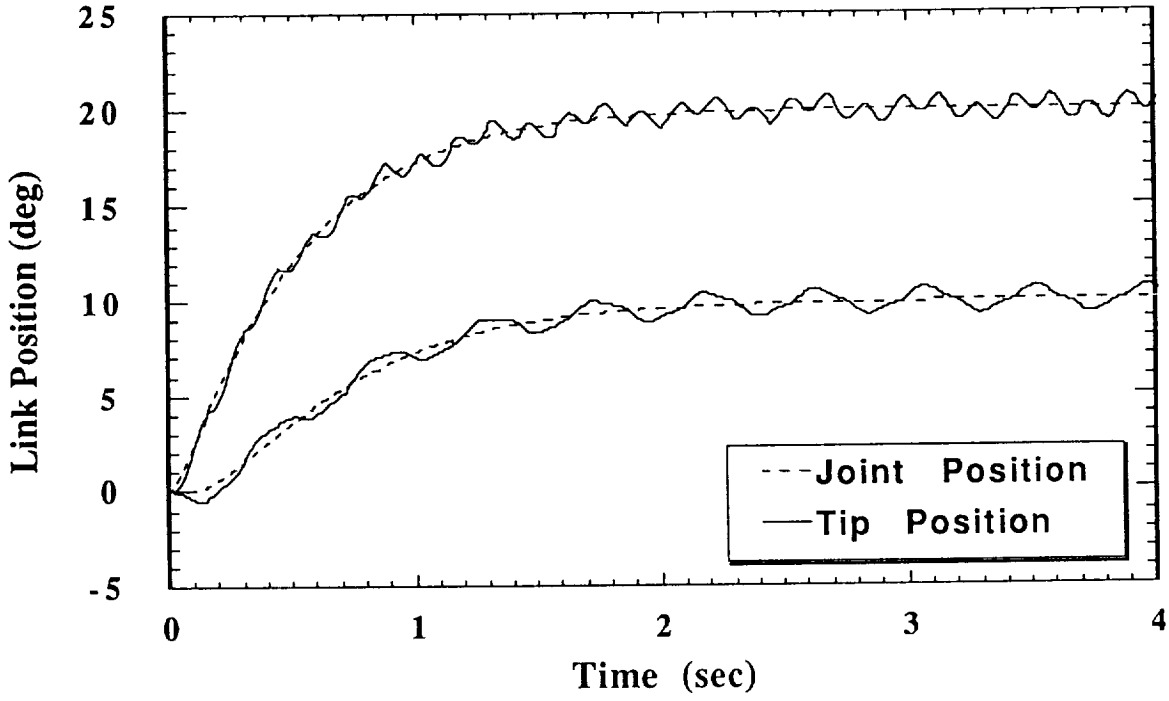

Figure 12. Simulation of link position as a function of time for a typical move of a double link arm using conventional position and velocity feedback control.

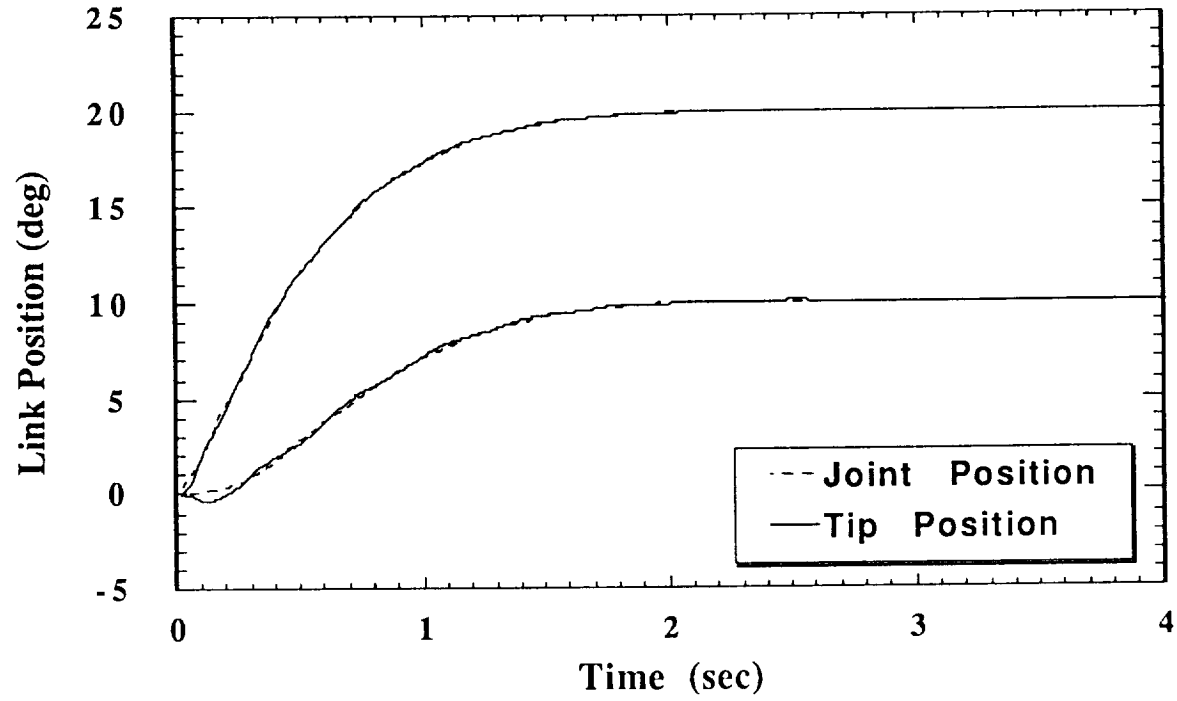

Figure 13. Simulation of link position as a function of time for a typical move of a double link arm using the new control system with deflection feedback control.

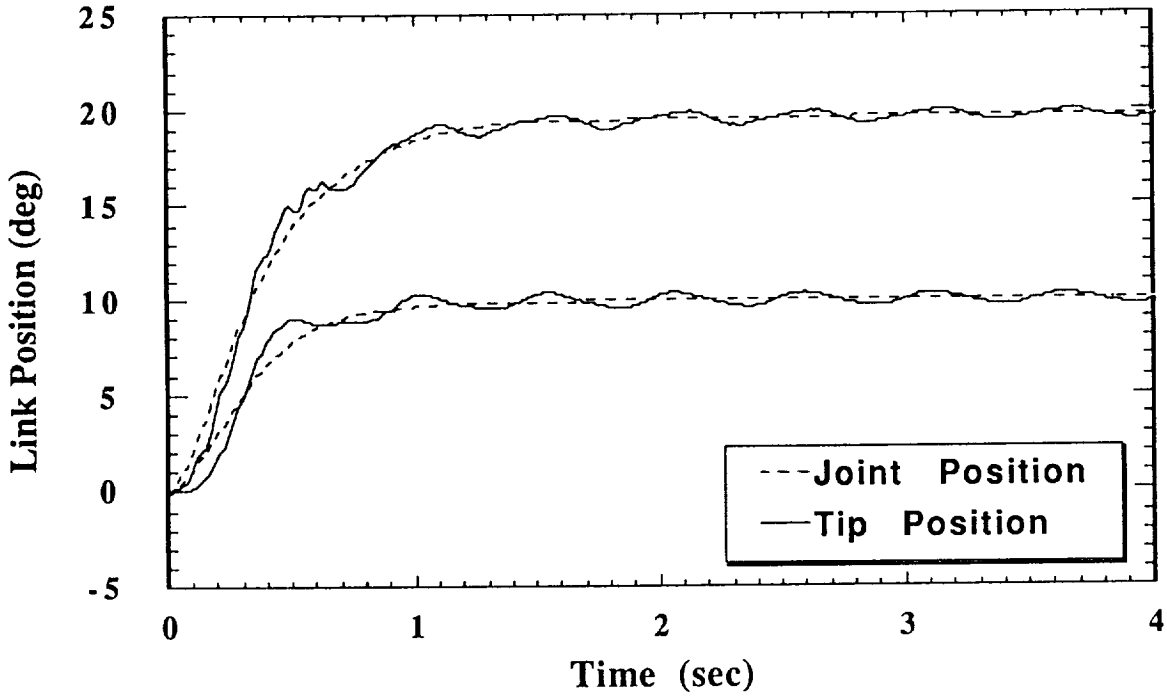

Figure 14. Experimental link position as a function of time for a typical move of the double link test arm using conventional position and velocity feedback control.

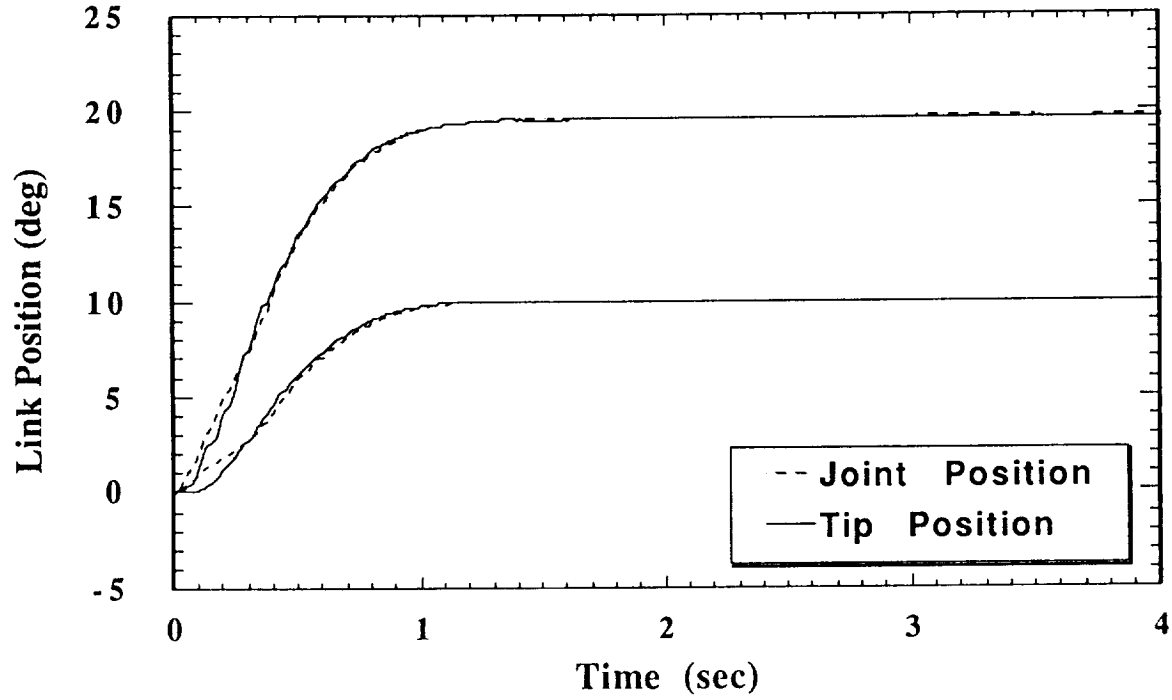

Figure 15. Experimental link position as a function of time for a typical move of the double link test arm using the new control system with deflection feedback.

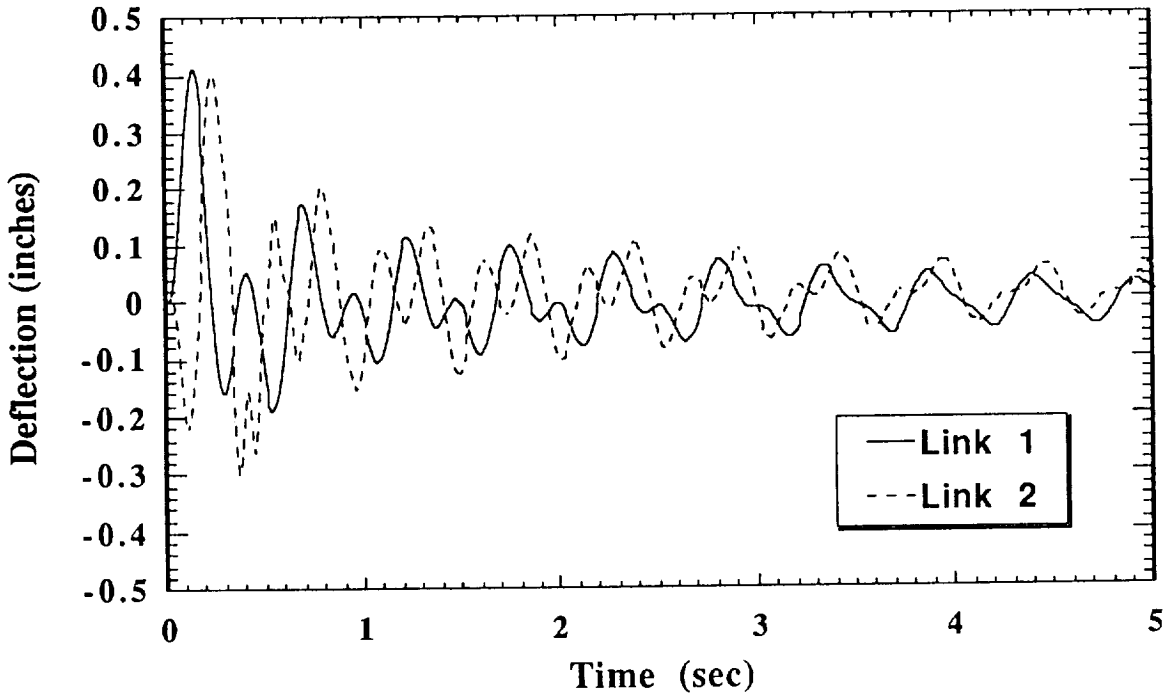

Figure 16. Experimental link deflection as a function of time for an impulse loading at the tip of the double link test arm using conventional position and velocity feedback control.

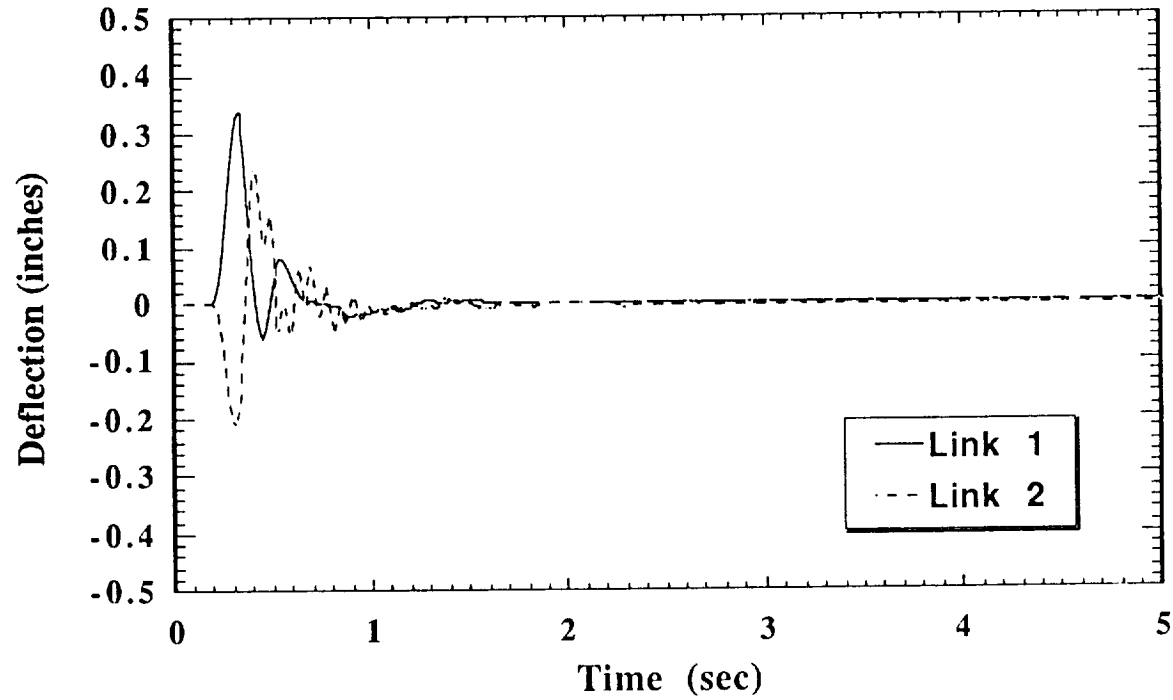

Figure 17. Experimental link deflection as a function of time for an impulse loading at the tip of the double link test arm using the new control system with deflection feedback.

6. Distribution List

NASA/MSFC — 1 copy
Attn: AP29-F
Marshall Space Flight Center, AL 35812

NASA/MSFC — 5 copies
Attn: CN22D
Marshall Space Flight Center, AL 35812

NASA/MSFC — 1 copy
Attn: AT01
Marshall Space Flight Center, AL 35812

NASA/MSFC — 1 copies
Attn: CC01/Wofford
Marshall Space Flight Center, AL 35812

NASA/MSFC — 1 copy
Attn: ER01/Haussler
Marshall Space Flight Center, AL 35812

NASA/MSFC — 1 copy
Attn: EM12A/Thompson
Marshall Space Flight Center, AL 35812

NASA/MSFC — 1 copy
Attn: EB24/William Jacobs
Marshall Space Flight Center, AL 35812
FAX: (205) 544-5864

NASA/MSFC — 6 copies
Attn: EB24/Hinman
Marshall Space Flight Center, AL 35812

NASA Scientific and Technical Information Facility — 2 copies
Attn: Accessioning Department
P. O. Box 8757
Baltimore/Washington International Airport, MD 21240